# Glycerol monooleate reverse micelles in nonpolar solvents

# Glycerol Monooleate Reverse Micelles in Nonpolar Solvents: Computer Simulations and Small-Angle Neutron Scattering

Joshua L. Bradley-Shaw,[†] Philip J. Camp,[*,†] Peter J. Dowding,[‡] and Ken Lewtas[†]

*School of Chemistry, University of Edinburgh, David Brewster Road, Edinburgh EH9 3FJ, Scotland, and Infineum UK Ltd, PO Box 1, Milton Hill, Abingdon OX13 6BB, UK*

E-mail: philip.camp@ed.ac.uk

February 24, 2015

[*]To whom correspondence should be addressed
[†]University of Edinburgh
[‡]Infineum UK Ltd

**Abstract**

The formation of glycerol monooleate reverse micelles in *n*-heptane and toluene at room temperature is studied using molecular-dynamics simulations and small-angle neutron scattering. The glycerol monooleate concentrations under consideration are in the range 1–20 wt%. Under these conditions, spontaneous reverse-micelle formation is observed on the simulation timescale (up to 30 ns). From simulations, the typical dimensions (semi-axes) of the equivalent ellipsoids with the same masses and moments of inertia are in the range 15–23 Å, with instantaneous shapes that are slightly nonspherical. By analyzing the scattering form factors from simulation and experiment, the radii of gyration of the reverse micelles are determined to be approximately 15 Å. The number of glycerol monooleate molecules in a reverse micelle is smaller in toluene ($\sim 20$) than in *n*-heptane ($\sim 30$) but the overall dimensions are similar due to greater penetration of the toluene in to the reverse micelle. The effects of low concentrations (1 wt%) of water, acetic acid, and ethanol on the reverse-micelle dimensions are determined. The overall structural effects are small, but the distributions of the molecules within the reverse micelles are shown to be sensitive to the molecular polarity.

# 1 Introduction

Surfactant molecules may form reverse micelles (RMs) when dispersed in nonpolar liquids, and particularly in the presence of small amounts of water. In a RM, the surfactant polar head groups are shielded from the nonpolar environment by the surfactant nonpolar tail groups. The interior of the RM may accommodate water molecules, which means that it can be used as a 'microreactor'.[1] One of the most intensively studied RM forming systems is the anionic surfactant sodium *bis*-(2-ethylhexyl)sulfosuccinate, known as Aerosol OT (AOT), dispersed in water/alkane mixtures. This system has been used for crystallization,[2] protein extraction, and particle synthesis.[3,4] The existence or not of a well-defined critical (reverse) micelle concentration (CMC) has been debated. The clustering of surfactants in nonpolar solvents was predicted to increase only very gradually with concentration,[5] It has been suggested that the presence of water is necessary for a CMC,[6] and that in dry non-polar solvents, AOT might aggregate until it comes out of solution.[7] Recent small-angle neutron scattering (SANS) measurements on AOT in almost completely dry cyclohexane show a clear CMC.[8]

The addition of water to surfactant-in-oil systems may have a significant effect on the shapes of the RMs. For instance, lecithins in $CHCl_3$/MeOH/$H_2O$ mixtures undergo a sphere-to-rod transition with increasing water content, with the wormlike micelles ultimately entangling and forming an organogel.[9–11] As another example, the addition of water to nickel(II) *bis*-(2-ethylhexyl)phosphate in *n*-hexane promotes the formation of quasi-one dimensional, rod-like RMs and water channels, although whether those channels are fully enclosed by the RMs is a matter of debate.[12]

Glycerol monooleate (GMO) is a widely used non-ionic surfactant and friction modifier. When dispersed in nonpolar solvents, GMO may self-assemble to form reverse micelles (RMs), with the polar glycerol head groups shielded from the nonpolar solvent by the aliphatic tail of the oleate moiety. (Note that the self-assembly and phase behavior of GMO in water is also known.[13]) In recent experimental work, Shrestha *et al.* examined the structures of GMO RMs in various alkanes using small-angle X-ray scattering (SAXS) and rheometric measurements.[14] It was found that at GMO concentrations of 5 wt%, the RMs resemble prolate ellipsoids, with major diameters that

range from 5.7 nm in *n*-hexane to 10 nm in *n*-hexadecane, while the other dimensions remained roughly constant, i.e., the RMs become more elongated with increasing solvent molecular weight. If a RM becomes more elongated, then its spontaneous curvature becomes less negative. The observed trend was therefore explained by the fact that larger alkanes are less able to penetrate in between the aliphatic tails of the surfactant,[15] leading to the spontaneous curvature becoming less negative. It was observed that small concentrations of water lead to significant enhancements in micelle size. The addition of 0.3 wt% water to 10 wt% GMO in *n*-decane was found to increase the major and minor diameters, respectively, from 8.0 nm to 12.4 nm (55% increase) and 2.5 nm to 3.2 nm (28% increase). Shrestha *et al.* write that, "It is most likely that some water molecules hydrate the surfactant so that the overall hydrophilic size of the surfactant increases and favors the micellar growth by reducing the [critical packing parameter]."[14] The closely related molecules glycerol dioleate, glycerol trioleate, and diglycerol monooleate are also known known to form RMs.[16] Increasing the size of the polar head group from glycerol monooleate to diglycerol monooleate leads to an increase in micelle size, while the addition of oleate tails leads to a decrease in micelle size. Other glycerol and diglycerol-based surfactants show similar qualitative trends.[17,18] In related work, Rappolt *et al.* examined the structures of cubic close-packed phases of fully hydrated RMs formed from binary mixtures of GMO (also called monoolein) and oleic acid, and the corresponding *trans* isomers glycerol monoelaidate and elaidic acid, using X-ray crystallography.[19] It was found that the distances between neighboring RMs were in the region of 12–14 Å, which gives a rough indication of the RM size. The water was found to form a core of roughly 3 Å in radius.

The formation of GMO RMs may be of high significance to its performance as a friction modifier. GMO is added to oils to tune viscosity and friction, but a detailed understanding of the molecular-scale structure and dynamics is lacking, and particularly near liquid-solid interfaces. What is clear is that the extent of GMO aggregation should strongly influence the tribological properties, and so the question of RM formation is an important one. In applications such as in engines, trace amounts of small polar molecules such as water (from combustion), ethanol (when

used as a biogasoline component), and acetic acid (AcOH, from breakdown products) may be present. As indicated above, such impurities can drive significant structural changes which might affect tribological properties. Therefore, the formation of RMs by molecules such as GMO in nonpolar solvents, and in the presence of small concentrations of polar molecules, is a subject worthy of study.

The focus of this article is the study of GMO RMs by molecular-dynamics (MD) simulation. From a modeling perspective, there have been far more simulation studies of micelle formation in aqueous systems than of RM formation in nonpolar solvents. Brown and Clarke were amongst the first to model reverse-micelle formation of a coarse-grained surfactant in nonpolar solvent and water.[20] Fully atomistic MD simulations have been used to study AOT in water/isooctane mixtures,[21–24] AOT in water/hexane mixtures,[25] and fluorinated surfactants in carbon dioxide/water mixtures.[26] Specific interest has focused on the properties of water in the interior of reverse micelles, modeled as an aqueous spherical core confined by surfactant.[27–34]

In the current work, MD simulations are used to study the spontaneous formation of RMs by GMO in two model oils (*n*-heptane and toluene) and the effects of small concentrations of water, AcOH, and EtOH. The dimensions of the RMs are estimated by analysis of the inertia tensor and by analyzing simulated form factors obtained from SANS. The distributions of the surfactant moieties and impurity molecules within the RMs are examined and correlated with the relative polarities. It is shown that the simulated RM dimensions compare reasonably well with those typically seen in the SAXS experiments of Shrestha *et al.*[14] The number of GMO molecules per RM is smaller in toluene than in *n*-heptane, but the characteristic dimensions of the RM are comparable; this is shown to be due to greater penetration of the toluene in to the RM, causing a swelling effect. The dimensions of the RMs are found to be roughly independent of GMO concentration when no small polar molecules are added. In the presence of small polar molecules, the RM size increases with increasing GMO concentration. At high GMO concentration, the addition of water or AcOH also leads to an increase in RM elongation. Water is the most polar impurity studied, and it remains tightly confined to the interior of the RM; EtOH is the least polar impurity studied, and

it is distributed more uniformly throughout the RM; AcOH is intermediate between the two.

To complement the simulation results, and the existing SAXS results of Shrestha *et al.*,[14] a small selection of SANS results are presented, confirming the formation of GMO RMs, and their basic dimensions. Both SANS measurements and MD simulations can be used to estimate the RM form factor, which can be fitted to obtain an estimate of the radius of gyration. The key point here, is that the same analysis protocol applied to both sets of data give roughly the same results for the radius of gyration of the RM.

The article is organized as follows. The details of the MD simulations and SANS measurements are given in section 2. The results are presented and discussed in section 3, and are organized in terms of RM formation in GMO/*n*-heptane and GMO/toluene mixtures (section 3.1), and then in the presence of small amounts of water, AcOH, or EtOH (section 3.2). Section 4 concludes the article.

# 2 Methods

## 2.1 Molecular dynamics

All-atom MD simulations were performed using LAMMPS.[35,36] Bulk-phase simulations were initiated from configurations in cubic boxes of side $L$ generated using Packmol.[37,38] Canonical ($NVT$) runs and isothermal-isobaric ($NPT$) runs were carried out using a Nosé-Hoover thermostat/barostat. In all cases, periodic boundary conditions were applied in all three directions, long-range Coulombic interactions (detailed below) were handled using the particle-particle-particle-mesh method, and the integration was carried out using the velocity Verlet algorithm with a timestep of 1 fs.

Preliminary bulk-phase $NPT$ simulations of $N = 500$ molecules of *n*-heptane or toluene were conducted using DREIDING,[39] OPLS-AA[40] (optimized for long-chain hydrocarbons[41]) and TraPPE[42–44] forcefields. All of the non-bonded interactions are described by a combination of Lennard-Jones (LJ) interactions (with the Lorenz-Berthelot mixing rules) and Coulombic interactions. Mass den-

sities ($\rho$) were measured at $P = 1$ atm and $T = 273$ K, 298 K, and 323 K, and compared to experimental data.[45] For *n*-heptane, these potentials gave $\rho = 435$ kg m$^{-3}$ (DREIDING), 597 kg m$^{-3}$ (OPLS-AA), and 669 kg m$^{-3}$ (TraPPE) at $T = 298$ K, as compared to the experimental value of 680 kg m$^{-3}$. For toluene, the corresponding simulated values were $\rho = 638$ kg m$^{-3}$ (DREIDING), 828 kg m$^{-3}$ (OPLS-AA), and 832 kg m$^{-3}$ (TraPPE) at $T = 298$ K, while the experimental value is 862 kg m$^{-3}$. The deviations between simulation and experiment were similar at lower and higher temperatures. TraPPE is therefore most accurate, but in the case of toluene, this forcefield is not parameterized with explicit hydrogens, while OPLS-AA is. All-atom simulations are required in this work, since it also deals with impurity molecules such as water. Therefore, even though it is less accurate than TraPPE in the case of *n*-heptane, OPLS-AA is used throughout for the solvent.

The initial conformation of an isolated GMO molecule was optimized with a density-functional calculation at the B3LYP 6-311+G(d,p) level using Gaussian 09;[46] the partial charges on the GMO atoms were taken from the same calculation. The LJ interaction parameters were taken from the OPLS-AA forcefield. The water molecules were described using the SPC/E model, while the AcOH and EtOH molecules were described using the OPLS-AA forcefield.

Mixtures of GMO, solvent (*n*-heptane or toluene), and impurity (water, acetic acid, or ethanol) were prepared at the desired compositions, and with total system sizes ranging from $N = 2975$ to $N = 48594$ atoms; see Table 1 for a summary. Each system was equilibrated at $T = 373$ K for 50 ps under $NVT$ conditions to yield a fully disordered configuration. Then the system was equilibrated at the target temperature of 298 K for 250 ps under $NVT$ conditions before switching to $NPT$ conditions with $P = 1$ atm. The $NPT$ simulations were run until the system had reached a steady state of aggregation, and this was typically achieved in less than 25 ns. Averages were measured over production runs of 5 ns after equilibration.

## 2.2 Small-angle neutron scattering

Small-angle neutron scattering experiments were performed on the NG7 30 m beamline at the National Institute of Standards and Technology's Center for Neutron Research (NCNR) in Gaithers-

Table 1: Compositions of the systems studied using MD simulation: $N_{\mathrm{GMO}}$ is the number of GMO molecules; $N_{\mathrm{s}}$ is the number of solvent molecules; $N_{\mathrm{i}}$ is the number of impurity molecules; $N_{\mathrm{a}}$ is the total number of atoms; and $\rho$ is the average equilibrium total mass density at $P = 1$ atm and $T = 298$ K; $L$ is the average simulation box length. Under 'Structure', 1RM means one RM, 2RM means two separate RMs, and C means a distribution of non-micellar GMO clusters, including single GMO molecules. In each case, the impurity (if present) is at 1 wt% concentration.

| wt% | $N_{\mathrm{GMO}}$ | Solvent | $N_{\mathrm{s}}$ | Impurity | $N_{\mathrm{i}}$ | $N_{\mathrm{a}}$ | $\rho$ / kg m$^{-3}$ | $L$ / Å | Structure |
|---|---|---|---|---|---|---|---|---|---|
| | | | | Pure | | | | | |
| 5 | 30 | *n*-heptane | 2028 | none | 0 | 48594 | 695 | 80.0 | 2RM |
| 10 | 30 | *n*-heptane | 961 | none | 0 | 24053 | 707 | 63.1 | 1RM |
| 20 | 15 | *n*-heptane | 213 | none | 0 | 5874 | 723 | 39.4 | C |
| 20 | 20 | *n*-heptane | 285 | none | 0 | 7855 | 721 | 43.5 | C |
| 20 | 30 | *n*-heptane | 427 | none | 0 | 11771 | 724 | 49.7 | 1RM |
| 20 | 35 | *n*-heptane | 499 | none | 0 | 13752 | 726 | 52.3 | C+1RM |
| 20 | 40 | *n*-heptane | 570 | none | 0 | 15710 | 717 | 54.9 | C+1RM |
| 20 | 60 | *n*-heptane | 855 | none | 0 | 23542 | 720 | 62.7 | 2RM |
| 5 | 20 | toluene | 1470 | none | 0 | 23350 | 836 | 65.7 | 1RM |
| 10 | 20 | toluene | 697 | none | 0 | 11755 | 831 | 52.2 | 1RM |
| 20 | 10 | toluene | 155 | none | 0 | 2975 | 842 | 32.8 | C |
| 20 | 15 | toluene | 232 | none | 0 | 4455 | 843 | 37.5 | C |
| 20 | 20 | toluene | 310 | none | 0 | 5950 | 841 | 41.3 | 1RM |
| 20 | 25 | toluene | 388 | none | 0 | 7430 | 842 | 44.5 | C+1RM |
| 20 | 40 | toluene | 620 | none | 0 | 11900 | 840 | 52.1 | 2RM |
| | | | | $H_2O$ impurity | | | | | |
| 5 | 30 | *n*-heptane | 2007 | $H_2O$ | 119 | 48468 | 710 | 79.4 | C+1RM |
| 10 | 30 | *n*-heptane | 952 | $H_2O$ | 60 | 24026 | 711 | 63.0 | 1RM |
| 20 | 30 | *n*-heptane | 422 | $H_2O$ | 30 | 11755 | 732 | 49.5 | 1RM |
| 10 | 20 | toluene | 690 | $H_2O$ | 40 | 11770 | 840 | 52.1 | 1RM |
| 20 | 20 | toluene | 306 | $H_2O$ | 20 | 5950 | 843 | 41.3 | 1RM |
| | | | | AcOH impurity | | | | | |
| 10 | 30 | *n*-heptane | 952 | AcOH | 18 | 23990 | 717 | 62.8 | 1RM |
| 20 | 30 | *n*-heptane | 422 | AcOH | 9 | 11728 | 737 | 49.4 | 1RM |
| 10 | 20 | toluene | 690 | AcOH | 12 | 11746 | 840 | 52.1 | 1RM |
| 20 | 20 | toluene | 306 | AcOH | 6 | 5938 | 850 | 41.2 | 1RM |
| | | | | EtOH impurity | | | | | |
| 10 | 30 | *n*-heptane | 952 | EtOH | 24 | 24062 | 711 | 63.0 | 1RM |
| 20 | 30 | *n*-heptane | 422 | EtOH | 12 | 11764 | 730 | 49.6 | 1RM |
| 10 | 20 | toluene | 690 | EtOH | 16 | 11794 | 837 | 52.1 | C+1RM |
| 20 | 20 | toluene | 306 | EtOH | 8 | 5962 | 847 | 41.2 | 1RM |

burg, MD, USA.[47] Samples of glycerol monooleate (Aldrich, $> 99\%$) were prepared using deuterated toluene (Goss Scientific, 99.6%) or deuterated *n*-heptane (Goss Scientific, 98%). The use

of deuterated solvents provided contrast for neutrons to elucidate self-assembled structures of GMO. Samples were run using 5 mm pathlength quartz cuvettes in a temperature-controlled sample holder. A sample to detector distance of 1.8 m was used with a neutron wavelength of 8 Å to obtain a $q$ range of 0.0011–0.2524 $\text{Å}^{-1}$. The scattered intensity $I(q)$ was obtained by circular averaging of the intensity.

# 3 Results and discussion

Results are presented first for GMO in pure solvents (section 3.1) and then the effects of impurities are considered (section 3.2).

## 3.1 GMO in *n*-heptane or toluene

Simulations of 5 wt%, 10 wt%, and 20 wt% GMO in *n*-heptane and toluene were carried out with various system sizes as given in Table 1. To begin with, solutions of GMO in solvents without impurities were surveyed to try and establish RM formation and the characteristic number of GMO molecules per RM. Table 1 shows results for 20 wt% GMO in *n*-heptane and toluene, with different numbers of GMO molecules (at the same concentration). (This was done at high GMO concentration in order to minimize the computational burden of including large numbers of solvent molecules.) Using a Goldilocks principle, if the number of GMO molecules was 'just right', then one or two well-defined RMs could be observed in the system, with no free GMO or small GMO clusters. If the number of GMO molecules was too small to form one RM, then only small clusters and monomers could be observed. If the number of GMO molecules was too small to form two RMs, then one RM was seen to coexist with small clusters and monomers. These various outcomes were easily identified by direct visualization of simulation configurations, and some examples are shown in Figure 1. The results are summarized in Table 1 as C (small clusters and monomers), 1RM or 2RM (one RM or two separate RMs), or C+1RM (small clusters and monomers, and one RM). For *n*-heptane, the optimum number of GMO molecules per RM was 30 for 10 wt% and

20 wt% GMO systems. The 5 wt% system (shown in Figure 1a) gave two large aggregates of approximately 15 GMO molecules. In toluene, the optimum RM size is 20 GMO molecules at all concentrations. Simulation snapshots of RMs in systems at various GMO concentrations are shown in Figure 1. A simulation movie of the self-assembly process is provided in the Supporting Information. Movie 1 shows 10 wt% GMO in pure *n*-heptane without impurity. The movie begins with a disordered configuration of GMO and solvent, and then shows the aggregation of the GMO to form a single RM over a period of 20 ns.

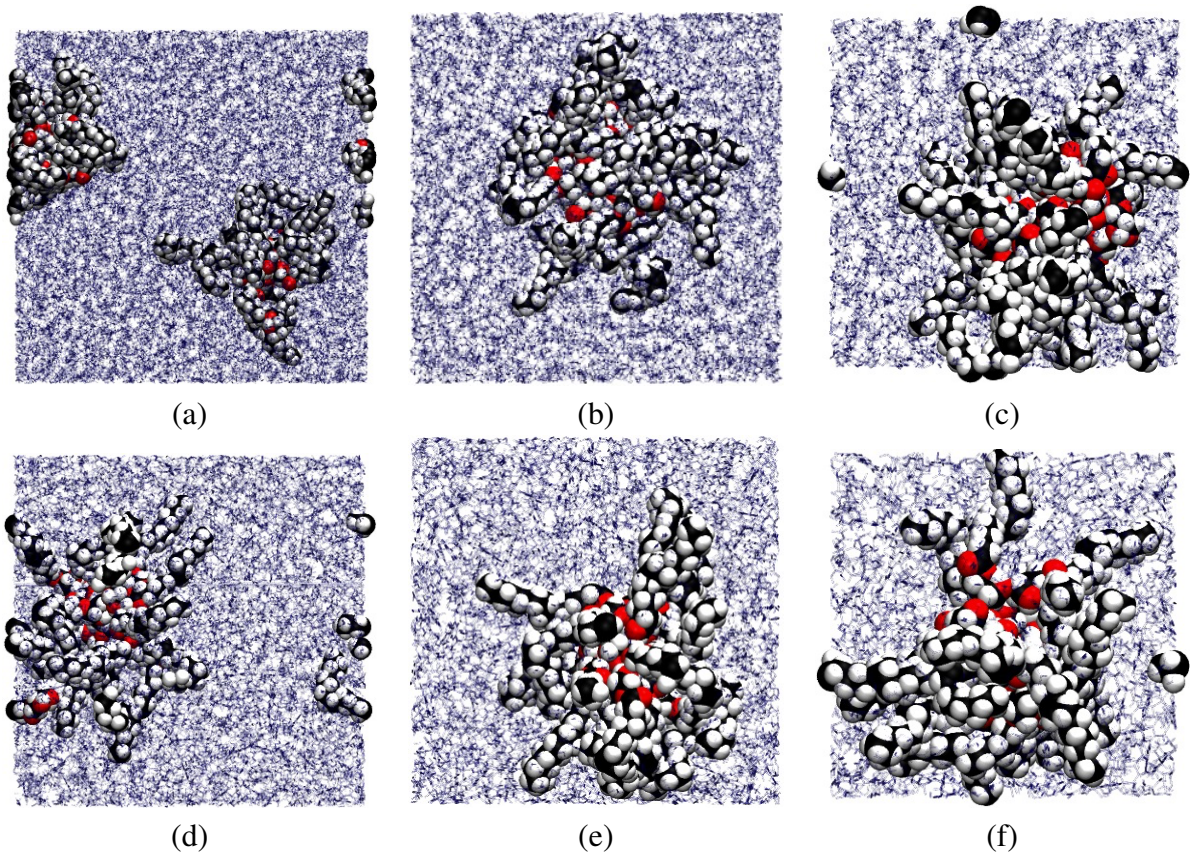


Figure 1: Simulation configurations at the end of 10 ns runs: (a) 5 wt% GMO in *n*-heptane; (b) 10 wt% GMO in *n*-heptane; (c) 20 wt% GMO in *n*-heptane; (d) 5 wt% GMO in toluene; (e) 10 wt% GMO in toluene; (f) 20 wt% GMO in toluene.

The shape and size of a RM were characterized by the equivalent ellipsoid with semi-axes $a < b < c$, and of uniform mass density, that has the same mass and moments of inertia as the simulated RM. The inertia tensor $\boldsymbol{I}$ was calculated including all atoms in the RM, meaning those atoms in GMO and any impurity. First, the center of mass (COM) of the RM was determined with

due account of the periodic boundary conditions. The COM satisfies the relation

$$\sum_{i=1}^{N} m_i \left[ x_i - x_{\mathrm{COM}} - L_x W \left( \frac{x_i - x_{\mathrm{COM}}}{L_x} \right) \right] = 0 \tag{1}$$

where $x_i$ is the $x$ coordinate of particle $i$, $x_{\mathrm{COM}}$ is the $x$ coordinate of the COM, $W(t)$ returns the nearest whole number to $t$, and the quantity in square brackets is the minimum-image separation between particle $i$ and the COM. The COM was obtained by a simple iteration

$$x'_{\mathrm{COM}} = \frac{\sum_{i=1}^{N} m_i \left[ x_i - L_x W \left( \frac{x_i - x_{\mathrm{COM}}}{L_x} \right) \right]}{\sum_{i=1}^{N} m_i} \tag{2}$$

with an initial guess $x_{\mathrm{COM}} = \sum_{i=1}^{N} m_i x_i / \sum_{i=1}^{N} m_i$, which may occur outside of the RM if the true COM is near the edge of the simulation box. In practice, less than 10 iterations were required for convergence. Similar expressions were solved in the $y$ and $z$ directions. $\boldsymbol{I}$ is given by

$$\boldsymbol{I} = \sum_{i=1}^{N} m_i \left[ (\boldsymbol{r}_i \cdot \boldsymbol{r}_i) \mathbf{1} - \boldsymbol{r}_i \otimes \boldsymbol{r}_i \right] \tag{3}$$

where $\boldsymbol{r}_i$ is the minimum-image vector between particle $i$ and the COM, and $\mathbf{1}$ is the unit tensor. Diagonalizing this tensor gives three eigenvalues $I_a > I_b > I_c$, which are the moments of inertia about the principal axes of the RM. The semi-axes of the equivalent ellipsoid with uniform mass density and total mass $M = \sum_{i=1}^{N} m_i$ are given by

$$a = \sqrt{\frac{5(I_b + I_c - I_a)}{2M}} \tag{4}$$

$$b = \sqrt{\frac{5(I_c + I_a - I_b)}{2M}} \tag{5}$$

$$c = \sqrt{\frac{5(I_a + I_b - I_c)}{2M}}. \tag{6}$$

These quantities were averaged over the last 5 ns of the simulation, and the results are summarized in Table 2. Note that $a$, $b$, and $c$ always represent the smallest, intermediate, and largest

semi-axes, respectively, and so these values measure the extent of nonspherical fluctuations in RM shape. In *n*-heptane at 10 wt% and 20 wt%, the RM dimensions are $a \simeq 15$–$16$ Å, $b \simeq 18$–$19$ Å, and $c \simeq 22$–$23$ Å. The results obtained by Shrestha *et al.* for 10 wt% GMO in *n*-hexane give $c \simeq 26$ Å, and the other two dimensions are estimated by them to be $a = b \simeq 12$ Å.[14] The number of GMO molecules in the RMs studied by Shrestha *et al.* can be estimated very roughly from the relative molecular mass and mass density of GMO (0.359 kg mol$^{-1}$ and $\rho = 970$ kg m$^3$, respectively) and the volume of the RM ($4\pi abc/3$), giving 27 molecules. The number of GMO molecules per RM studied in the simulations is therefore consistent with experiment, notwithstanding the small difference arising from different solvents.

Table 2: Dimensions of the equivalent ellipsoids of simulated RMs. $a$, $b$, and $c$ are the semi-axes of the ellipsoids, $R_g$ is the radius of gyration defined in eq 7, and $\kappa^2$ is the relative shape anisotropy defined in eq 8.

| wt% | Solvent | Impurity | $a$/Å | $b$/Å | $c$/Å | $b/a$ | $c/a$ | $R_g$/Å | $\kappa^2$ |
|---|---|---|---|---|---|---|---|---|---|
| | | | | Pure | | | | | |
| 5 | *n*-heptane | none | 13.1 | 15.8 | 18.6 | 1.21 | 1.42 | 12.5 | 0.043 |
| 10 | *n*-heptane | none | 15.8 | 18.0 | 23.1 | 1.14 | 1.46 | 14.9 | 0.055 |
| 20 | *n*-heptane | none | 15.5 | 19.0 | 21.8 | 1.23 | 1.41 | 14.7 | 0.038 |
| 5 | toluene | none | 17.6 | 22.6 | 28.5 | 1.28 | 1.62 | 18.1 | 0.053 |
| 10 | toluene | none | 16.6 | 20.1 | 24.7 | 1.22 | 1.49 | 16.1 | 0.058 |
| 20 | toluene | none | 16.8 | 20.4 | 24.2 | 1.22 | 1.44 | 16.0 | 0.047 |
| | | | | $H_2O$ impurity | | | | | |
| 10 | *n*-heptane | $H_2O$ | 15.2 | 18.3 | 23.4 | 1.21 | 1.54 | 14.9 | 0.064 |
| 20 | *n*-heptane | $H_2O$ | 13.9 | 16.4 | 30.7 | 1.18 | 2.20 | 16.8 | 0.258 |
| 10 | toluene | $H_2O$ | 16.0 | 18.0 | 20.1 | 1.13 | 1.25 | 14.0 | 0.021 |
| 20 | toluene | $H_2O$ | 15.0 | 18.0 | 21.1 | 1.20 | 1.41 | 14.1 | 0.041 |
| | | | | AcOH impurity | | | | | |
| 10 | *n*-heptane | AcOH | 15.6 | 17.6 | 26.9 | 1.12 | 1.72 | 16.0 | 0.128 |
| 20 | *n*-heptane | AcOH | 17.8 | 21.4 | 30.7 | 1.20 | 1.72 | 18.5 | 0.119 |
| 10 | toluene | AcOH | 16.0 | 18.4 | 22.1 | 1.16 | 1.37 | 14.7 | 0.040 |
| 20 | toluene | AcOH | 15.8 | 18.1 | 20.1 | 1.15 | 1.27 | 14.0 | 0.021 |
| | | | | EtOH impurity | | | | | |
| 10 | *n*-heptane | EtOH | 16.3 | 18.7 | 24.0 | 1.15 | 1.47 | 15.4 | 0.056 |
| 20 | *n*-heptane | EtOH | 16.9 | 19.7 | 22.1 | 1.16 | 1.31 | 15.3 | 0.025 |
| 10 | toluene | EtOH | 13.3 | 16.4 | 20.6 | 1.23 | 1.55 | 13.2 | 0.064 |
| 20 | toluene | EtOH | 15.4 | 17.0 | 18.6 | 1.10 | 1.20 | 13.2 | 0.012 |

Table 2 reports some other geometrical measures for the RMs. The radius of gyration $R_g$ for

an ellipsoid is given by

$$R_g^2 = \frac{a^2 + b^2 + c^2}{5}. \tag{7}$$

The radius of gyration can also be extracted by analyzing the form factor measured in SANS/SAXS experiments, and this is discussed below. The relative shape anisotropy is given by[48,49]

$$\kappa^2 = 1 - \frac{3I_2}{I_1^2} \tag{8}$$

where $I_1 = I_a + I_b + I_c$ and $I_2 = I_a I_b + I_b I_c + I_c I_a$: $\kappa^2 = 0$ for a sphere and $\kappa^2 = 1$ for a linear chain of particles. Typically, the boundary between spheres and rods is taken to be around $\kappa^2 = 0.05$. In all cases, $\kappa^2 \simeq 0.05$ for GMO in pure solvent, indicating moderately nonspherical RMs.

One indicator of the average RM size is the radius of gyration of the equivalent ellipsoid, $R_g$, defined by eq 7 and reported in Table 2. The results show that for a given wt%, the RMs in toluene and in *n*-heptane are comparable in size. (This can also be shown by calculating the volume of the equivalent ellipsoid, $4\pi abc/3$.) The apparent RM size is correlated with the degree of penetration of the solvent in to the hydrophobic part of the RM: although more solvent penetration should be associated with the spontaneous curvature becoming more negative, which should correspond to a smaller RM, the swelling effect of the solvent is actually dominant. This is because of the relatively small size of the RM (as compared to micelles in aqueous media) and the broad interface between GMO and solvent. It is not immediately obvious, *a priori*, which of the two solvents should penetrate better. Figure 2 shows the local densities of GMO and solvent as functions of radial distance $r$ from the COM of the RM, for systems at 10 wt% and 20 wt% GMO in *n*-heptane and toluene. Firstly, each of these figures shows that the solvent density profile tends toward the simulated bulk density at large $r$ (597 kg m$^{-3}$ and 828 kg m$^{-3}$ for *n*-heptane and toluene, respectively). Secondly, the local density of GMO in the core of the RM (at say $r < 5$ Å) is much higher in the *n*-heptane system than in the toluene system. (Note that the density profiles are expected to be noisy at low values of $r$, since the actual numbers of atoms are proportional to $4\pi r^2$.) Finally, the degree of overlap is greater for toluene than it is for *n*-heptane: the toluene

density profile penetrates the RM to a radius of $r = 5$ Å or less, while the *n*-heptane density profile only reaches to $r = 7$–8 Å. These observations indicate that toluene penetrates more than *n*-heptane in to the RM. Hence, although the RM contains fewer GMO molecules in toluene ($\sim 20$) than in *n*-heptane ($\sim 30$), the equivalent ellipsoids in *n*-heptane and toluene are comparable in size due to solvent penetration and swelling.

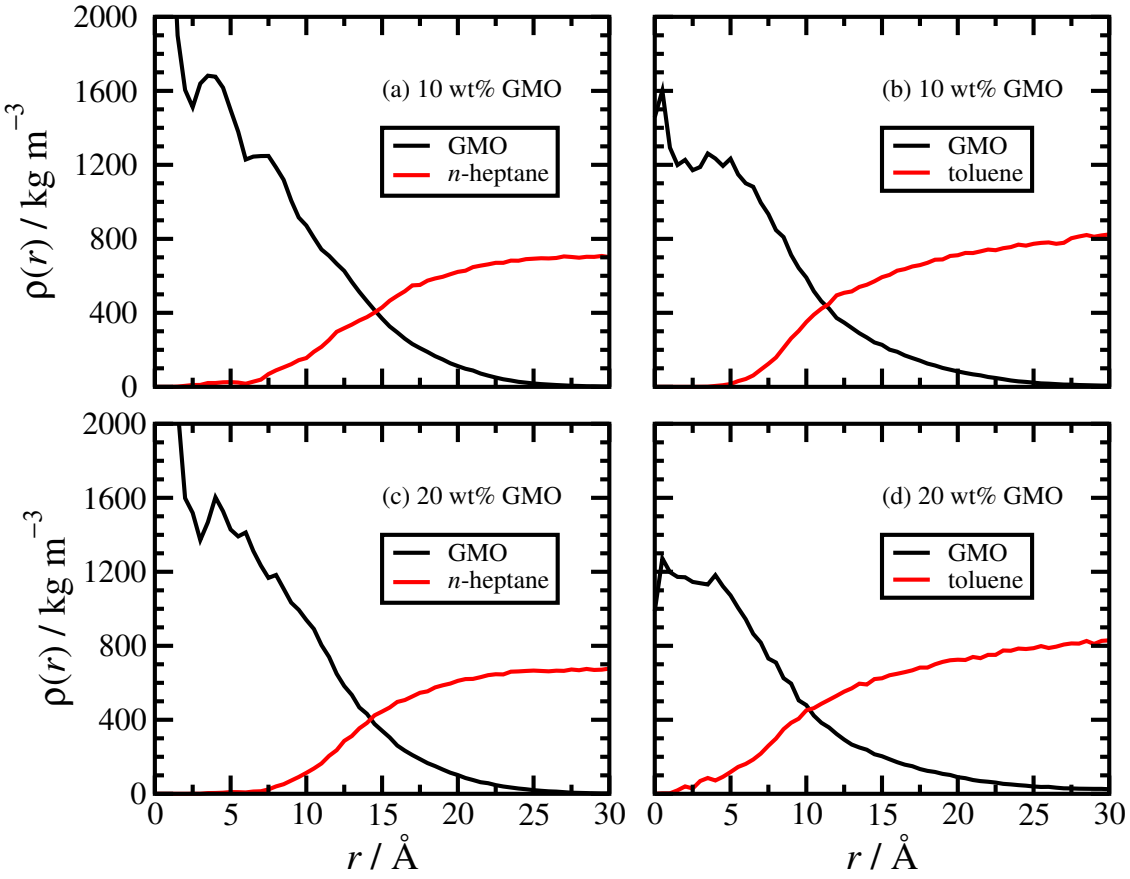


Figure 2: Mass density profiles $\rho(r)$ as functions of the radial distance $r$ from the RM center of mass, for 10 wt% GMO in (a) *n*-heptane and (b) toluene, and for 20 wt% GMO in (c) *n*-heptane and (d) toluene.

Figure 3 shows the form factors, $P(q)$, from SANS experiments for some selected systems. The use of deuterated solvents means that $P(q)$ can be fitted with models for the GMO RM. It proved impossible to fit the usual form-factor models (for solid bodies, core-shell structures, etc.) with any confidence. Figure 2 shows that the interface between GMO and solvent is quite broad, and so this should be incorporated in to a 'diffuse profile' fitting model. Two convenient choices

of GMO density profile are isotropic Gaussian and exponential functions.

$$\rho(r) = \rho(0)\exp(-\alpha^2 r^2) \quad \text{(Gaussian)} \tag{9}$$

$$\rho(r) = \rho(0)\exp(-\alpha r) \quad \text{(exponential)} \tag{10}$$

The radii of gyration for these density profiles are given by $R_g^2 = 3/2\alpha^2$ (Gaussian) and $R_g^2 = 12/\alpha^2$ (exponential). The form factor $P(\boldsymbol{q})$ is proportional to $|f(\boldsymbol{q})|^2$ where $f(\boldsymbol{q}) = \int \rho(\boldsymbol{r})\exp(-i\boldsymbol{q}\cdot\boldsymbol{r})\mathrm{d}\boldsymbol{r}$. Assuming that the structure factor $S(\boldsymbol{q}) = 1$ (no correlations between micelles) then the scattering intensity is proportional to $P(\boldsymbol{q})$. For isotropic density profiles, the form factor depends only on $q = |\boldsymbol{q}|$. The scattering intensities (normalized by the zero-wavevector values) for the Gaussian and exponential density profiles are as follows.

$$\frac{I(q)}{I(0)} = \exp\left(-\frac{q^2}{2\alpha^2}\right) = \exp\left(-\frac{q^2 R_g^2}{3}\right) \quad \text{(Gaussian)} \tag{11}$$

$$\frac{I(q)}{I(0)} = \left(1+\frac{q^2}{\alpha^2}\right)^{-4} = \left(1+\frac{q^2 R_g^2}{12}\right)^{-4} \quad \text{(exponential)} \tag{12}$$

Note that the low-wavevector Guinier approximation $I(q)/I(0) \approx 1 - q^2 R_g^2/3$ is observed in each case. The experimental total scattering intensity was fitted over the range $0.01\ \text{Å}^{-1} \le q \le 0.25\ \text{Å}^{-1}$ using the equation $I(q) = \Delta I + I(0)P(q)$, where $\Delta I$ is a background offset. In practice, the Gaussian and exponential fits to $I(q)$ gave very similar results. For instance, with 1 wt% GMO in *n*-heptane, the Gaussian fit gave $R_g = 16.30(6)$ Å while the exponential fit gave $R_g = 17.1(1)$ Å. A difference of less than one ångström is insignificant. In Figure 3, the experimental data are plotted in the form $P(q) = [I(q) - \Delta I]/I(0)$ using parameters from the Gaussian fits; the apparent values of $R_g$ are also shown. In general, the quality of the fit is excellent. The one exception is with 10 wt% GMO in *n*-heptane, where neither the Gaussian nor the exponential fit could get the correct behavior at low $q$. This could be due to the RMs being nonspherical and/or there being positional correlations between RMs [$S(q) \neq 1$]. Nonetheless, the fit is good in the range $q > 0.10\ \text{Å}^{-1}$, and the apparent $R_g$ is in good agreement with those at lower GMO concentrations, and so no further analysis

was carried out. A comparison of the experimental and simulated RM dimensions shows that simulations apparently underestimate $R_g$ in *n*-heptane, but overestimate $R_g$ in toluene. Note that the SANS data have only been analyzed in the crudest approximation, ignoring micellar correlations [$S(q) = 1$]. Nonetheless, the dimensions are roughly in agreement: at 10 wt%, the deviations between experiment and simulation are about 1 Å and 5 Å in *n*-heptane and toluene, respectively. Shrestha *et al.*'s estimates of $a = b \simeq 12$ Å and $c \simeq 26$ Å for 10 wt% GMO in *n*-hexane give, from eq 7, $R_g \simeq 14$ Å, which is in broad agreement with the experimental and simulation results presented here for *n*-heptane.

The simulated radii of gyration of RMs given in Table 2 were obtained by identifying the equivalent ellipsoids with equal masses and inertia tensors. $R_g$ can also be obtained by fitting a simulated form factor in exactly the same way as in experiment. Making the assumption that each atom in the simulated RM has an equal scattering cross section, the orientationally averaged form factor for a RM made up of $N$ atoms is

$$P(q) = \frac{1}{N^2} \sum_{i=1}^{N} \sum_{j=1}^{N} \left\langle \frac{\sin(qr_{ij})}{qr_{ij}} \right\rangle \tag{13}$$

where $r_{ij}$ is the separation between atoms $i$ and $j$ in a frame where the RM center of mass is at the origin, and with no periodic boundary conditions applied. With this definition, $P(0) = 1$ and the large-$q$ limit is $P(\infty) = 1/N$.

Figure 4 shows some examples of $P(q)$ from systems with 10 wt% and 20 wt% GMO, along with Gaussian fits (fitted over the same experimental range of $q \leq 0.25$ Å$^{-1}$) and the associated radii of gyration. Reassuringly, the values of $R_g$ are within 1–2 Å of the values for the equivalent ellipsoids, reported in Table 2. For the systems in *n*-heptane, the experimental and simulated form factors give values of $R_g$ within 2 Å of one another, while the experimental values in the toluene system are smaller than those measured in simulations. Of course, simulated data are available over an arbitrarily broad range of wavevectors. Here, the high-$q$ cutoff was set to $2\pi$ Å$^{-1}$, corresponding to real-space distances of 1 Å. To facilitate the comparison between simulation and

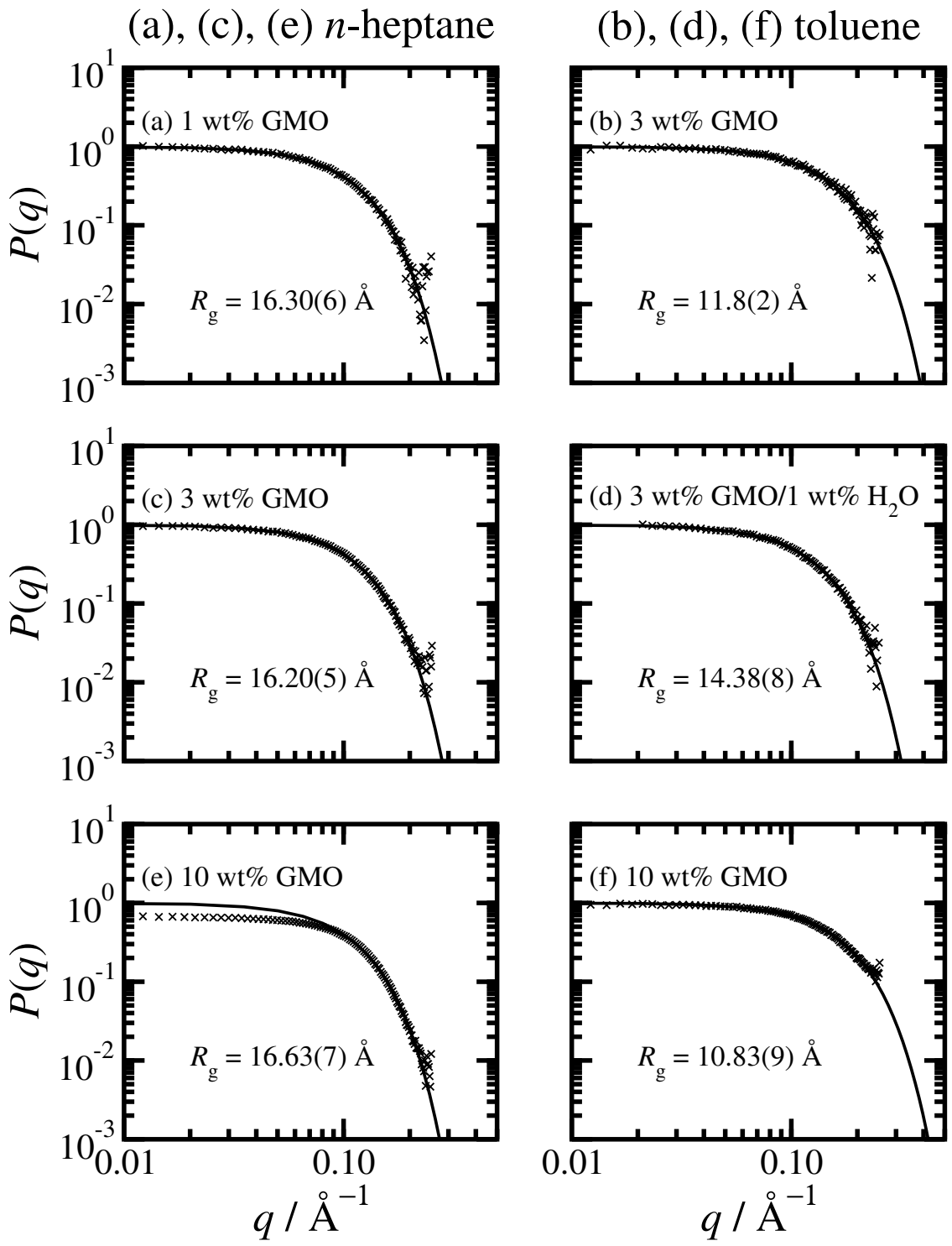


Figure 3: Experimental form factors $P(q)$ from SANS: (a) 1 wt% GMO in *n*-heptane; (b) 3 wt% GMO in toluene; (c) 3 wt% GMO in *n*-heptane; (d) 3 wt% GMO in toluene with 1 wt% $H_2O$; (e) 10 wt% GMO in *n*-heptane; (f) 10 wt% GMO in toluene. Experimental data are shown as crosses, the curves are fits using the Gaussian form factor (in the range 0.01 $\text{Å}^{-1} \leq q \leq 0.25$ $\text{Å}^{-1}$), and the corresponding values of $R_g$ are shown.

experiment, dotted lines in Figure 4 indicate the ranges over which the experimental data were plotted in Figure 3 [0.01 $\text{Å}^{-1} \leq q \leq 0.5$ $\text{Å}^{-1}$, $0.001 \leq P(q) \leq 10$]. The features at $q > 1$ $\text{Å}^{-1}$ correspond to real-space distances of less than about 6 Å, and so these are due to the short-range atomic ordering within the RM. The features in the intermediate range 0.3 $\text{Å}^{-1} < q < 1$ $\text{Å}^{-1}$ correspond to real-space distances of about 6–20 Å and so these arise from the conformations of the GMO chains in the interface between the RM and the surrounding solvent. In principle, these features should contain some useful information that could be used to derive improved fitting models for experimental form factors, but the range of wavevectors accessible to the current SANS experiments does not warrant it. The oscillations in $P(q)$ in the intermediate-$q$ range are reminiscent of those in well-known solid-body and core-shell form factors, but this is coincidental: the density profiles in Figure 2 show that the interface between the RM and the solvent is diffuse. Just as with the experimental data, it was impossible to fit any solid-body or core-shell form factors with confidence. In any case, the diffuse profiles expressed in eqs 11 and 12 were adequate for fitting the low-$q$ form factors from both SANS and simulation, and in a consistent way.

## 3.2 GMO in *n*-heptane or toluene with impurities

As explained in section 1, the addition of polar molecules to surfactant-in-oil systems can have a strong effect on the structural properties of RMs. In this section, the effects of added water, AcOH, and EtOH on GMO RMs are examined. These small molecules are amongst the most likely to be found as impurities in engine oils, and they span a broad range of polarity. The properties of 10 wt% GMO in solvents with 1 wt% impurity are considered first. System parameters are summarized in Table 1. The numbers of GMO molecules were kept fixed at 30 and 20 in *n*-heptane and toluene, respectively. A single RM was seen to form in all cases except for 10 wt% GMO in toluene with 1 wt% EtOH, which will be discussed further below. A simulation movie of the self-assembly process is provided in the Supporting Information. Movie 2 shows 10 wt% GMO in *n*-heptane with 1 wt% water. The movie begins with a disordered configuration of GMO, solvent, and impurity, and then shows the aggregation of the GMO to form a single RM over a

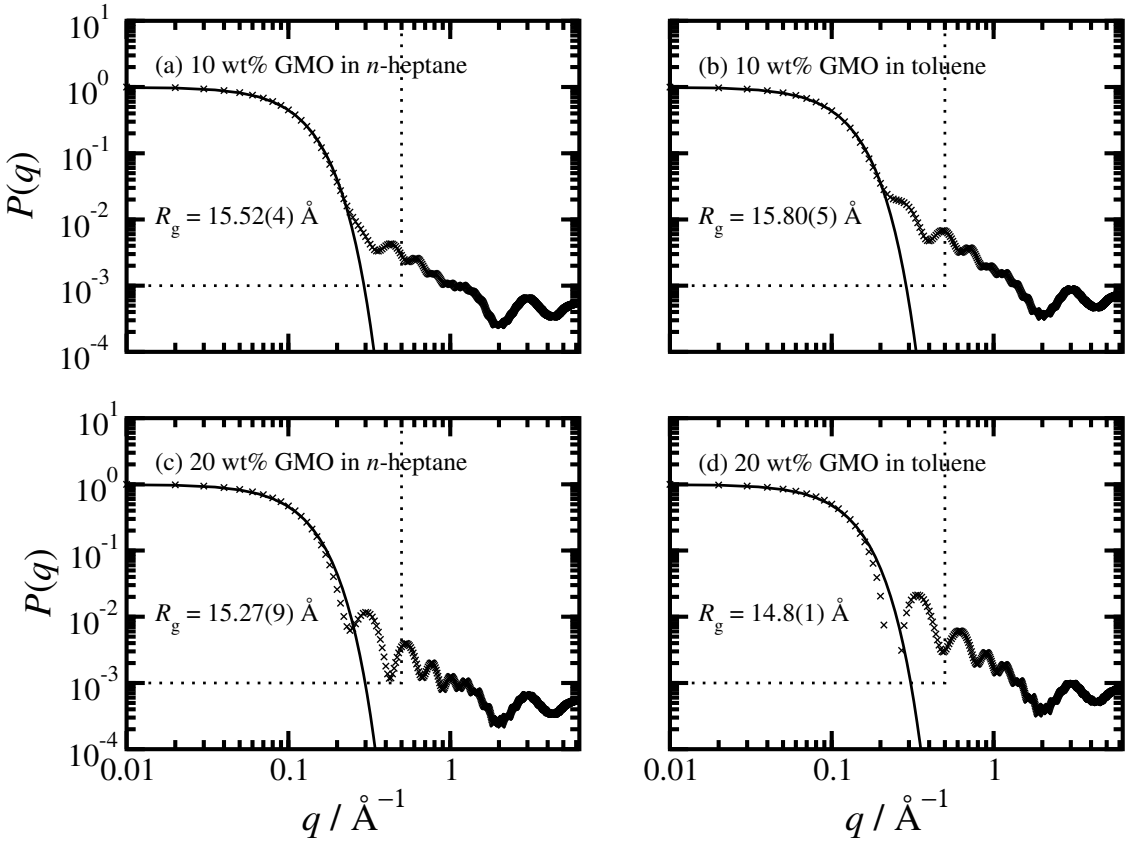


Figure 4: Simulated form factors $P(q)$ for GMO reverse micelles in pure solvents: (a) 10 wt% GMO in *n*-heptane; (b) 10 wt% GMO in toluene; (c) 20 wt% GMO in *n*-heptane; (d) 20 wt% GMO in toluene. Simulation data are shown as crosses, the curves are fits using the Gaussian form factor (in the range $q \leq 0.25$ Å$^{-1}$), and the corresponding values of $R_g$ are shown. The dotted lines indicate the same ranges of $q$ and $P(q)$ as shown in Figure 3.

period of 20 ns. The movie also shows the localization of the water in the centre of the RM.

Table 2 shows that the RM dimensions in the 10 wt% GMO systems are generally quite insensitive to the presence of impurities: the two minor semi-axes of the equivalent ellipsoids are in the region of $a = 16$ Å and $b = 18$ Å; the major axis is about $c = 23$ Å in all cases except AcOH, for which $c = 27$ Å. In practical terms, these dimensions are constant, but it's surprising nonetheless given how the impurity is distributed within the RMs. Figure 5 shows the mass-density profiles for GMO (at 10 wt%), solvent, and impurity (at 1 wt%) with respect to the RM center-of-mass. In toluene (Figure 5b) water impurity is strongly localized in the center of the RM, as expected. In *n*-heptane (Figure 5a) the water appears to be distributed more broadly throughout the RM, but in fact it forms more than one 'core' of water, around which the GMO molecules coordinate. A typical simulation snapshot is shown in Figure 6a; the three water cores are clearly visible. The RM dimensions ($R_g = 14$–$15$ Å) and the distribution of water within the RM are broadly in line with X-ray measurements on hydrated GMO/oleic acid RMs in cubic solid phases (RM size 12–14 Å and water-core radius 3 Å).[19]

AcOH molecules (Figures 5c and 5d) appear to form a dense core and a diffuse corona. Figures 5e and 5f show the EtOH profiles, and these are the most diffuse of all. The 'amphiphilic' behavior of small alcohols is well known,[50–52] and in this situation it leads to no strongly preferred location within the RM. Simulation snapshots of RMs in *n*-heptane with AcOH and EtOH impurities are shown in Figure 6b and 6c. The orientations of the AcOH and EtOH molecules are distributed almost isotropically. The probability distributions of the radial distances of the 'polar' carbon ($\underline{C}H_2OH$ in EtOH or $\underline{C}O_2H$ in AcOH) and the methyl carbon ($\underline{C}H_3$) from the RM center-of-mass (not shown) are both very close to the impurity density profiles in Figure 5, but with the polar distribution shifted to lower distances by about 1 Å.

A single RM is not clearly observed in the case of 10 wt% GMO in toluene with 1 wt% EtOH: see Figure 6d. Rather an ill-formed GMO aggregate was seen to coexist with smaller clusters. To check whether this was a reproducible result, repeat simulations were carried out, as well as heating and cooling cycles (between 298 K and 373 K) starting from equilibrated configurations.

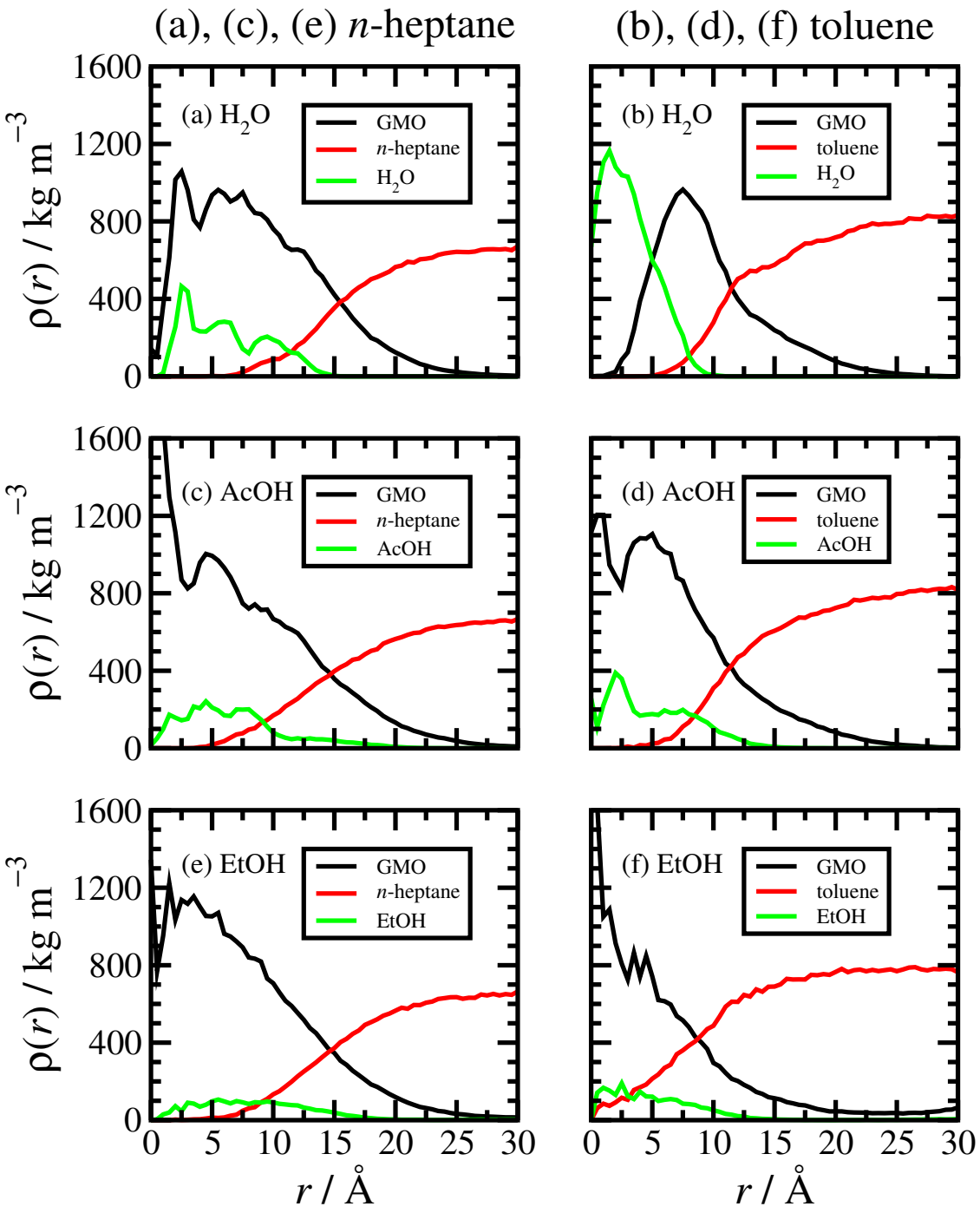


Figure 5: Mass density profiles $\rho(r)$ as functions of the radial distance $r$ from the RM center of mass for 10 wt% GMO systems in *n*-heptane (a, c, e) and toluene (b, d, f) with 1 wt% impurities ($H_2O$, AcOH, or EtOH): (a) and (b) $H_2O$; (c) and (d) AcOH; (e) and (f) EtOH.

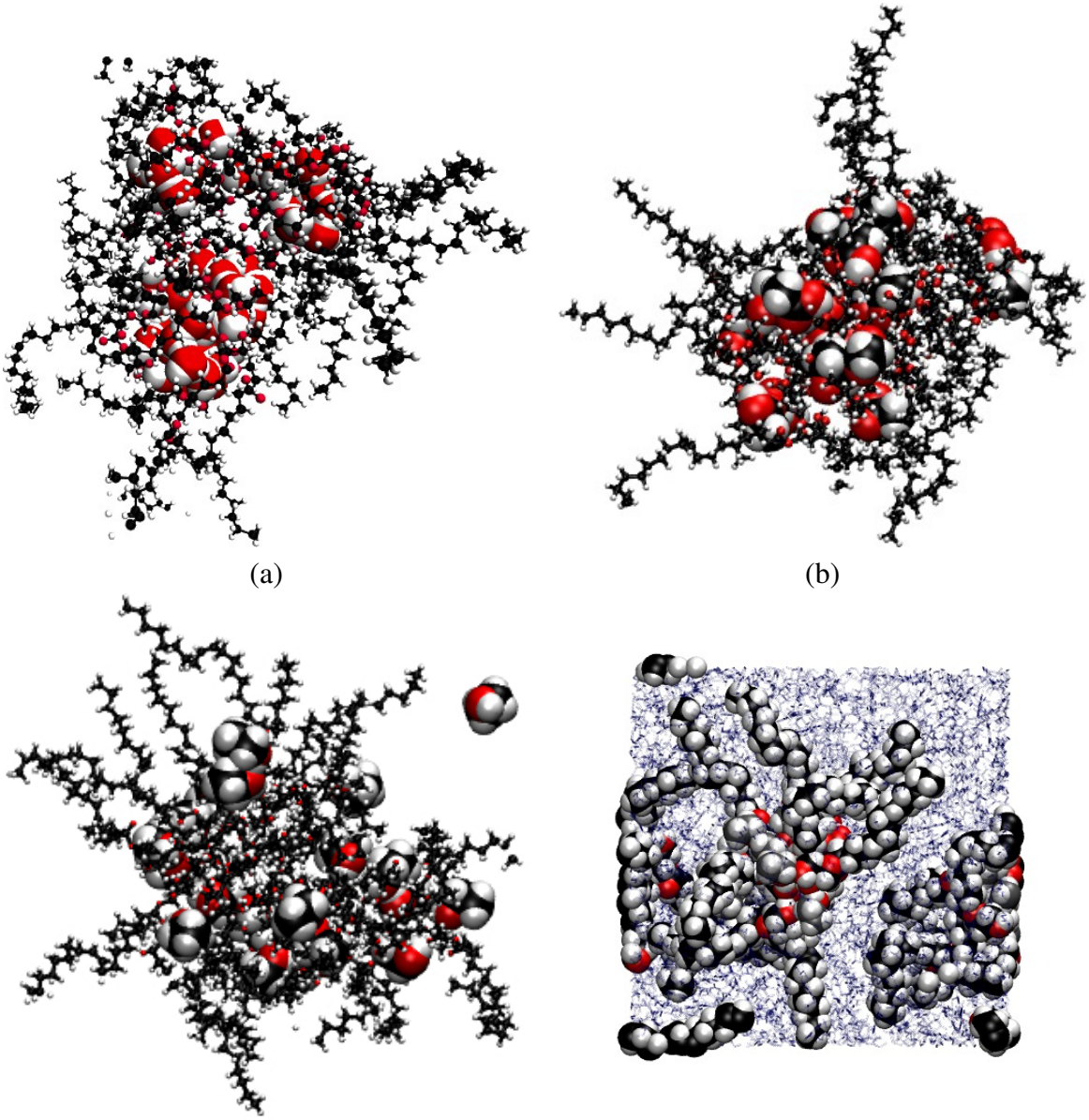

Figure 6: Simulation configurations at the end of 10 ns runs: (a) 10 wt% GMO in *n*-heptane with 1 wt% water; (b) 10 wt% GMO in *n*-heptane with 1 wt% AcOH; (c) 10 wt% GMO in *n*-heptane with 1 wt% EtOH (d) 10 wt% GMO in toluene with 1 wt% EtOH. In (a)-(c), only the GMO and impurity molecules are shown, and the atoms in the GMO molecules are shown reduced in size.

In all cases, the system at 298 K consisted of more than one cluster. For want of a better term, the largest cluster can be called a RM, but its radius of gyration is of course anomalously low – see Table 2. The density profiles of GMO, toluene, and EtOH can be calculated with respect to the center of mass of this cluster – see Figure 5f. Obviously, the GMO and EtOH profiles are less strongly localized than in the other cases.

Figure 7 shows the mass-density profiles for systems with 20 wt% GMO and various impurities (again at 1 wt%). A well-defined single RM is seen in every case. Ostensibly, the results are very similar to those of systems with 10 wt% GMO: water is strongly localized in the core of the RM, while the AcOH and EtOH are more broadly distributed. Table 2, however, shows that there are a couple of anomalous cases. The system with 20 wt% GMO and 1 wt% $H_2O$ in *n*-heptane has a very high value for $c \simeq 31$ Å, and correspondingly high values of $c/a \simeq 2.2$ and $\kappa^2 \simeq 0.26$, signaling a rod-like RM. The mass-density profile for GMO in Figure 7a shows a long tail, out to $r \simeq 30$ Å. Similarly, 20 wt% GMO in *n*-heptane with AcOH has high values of $c \simeq 31$ Å, $c/a \simeq 1.7$, and $\kappa^2 \simeq 0.12$, and the GMO density profile in Figure 7 has a very long tail. The elongations in both of these cases are so extreme, and the GMO concentrations are so high, that the major semi-axis is comparable in size to the simulation box length, so that the micelle actually spans the simulation box and interacts with its periodic images. This is not just a simulation artifact, however, because the RM size is also comparable to the average separation between RMs in an infinite system. What is not known is how the RMs merge with one another and form structures on lengthscales larger than the simulation box length. Therefore, there is not much that can be said about the true dimensions, or even the integrity, of RMs under these high-concentration conditions, except that the addition of water and AcOH may cause elongation of the RM on the 40–50 Å lengthscale. This is, nonetheless, in qualitative agreement with what is seen in experiment with GMO RMs in *n*-alkanes; Shrestha *et al.* observed a 55% increase in the major semi-axis upon addition of 0.3 wt% water to 10 wt% GMO in *n*-decane.[14] A systematic SANS investigation of impurity effects has not been carried out here, but it is noted that the apparent radius of gyration of RMs in 3 wt% GMO in toluene increases by about 2.6 Å on adding 1 wt% water; see Figures 3b and 3d.

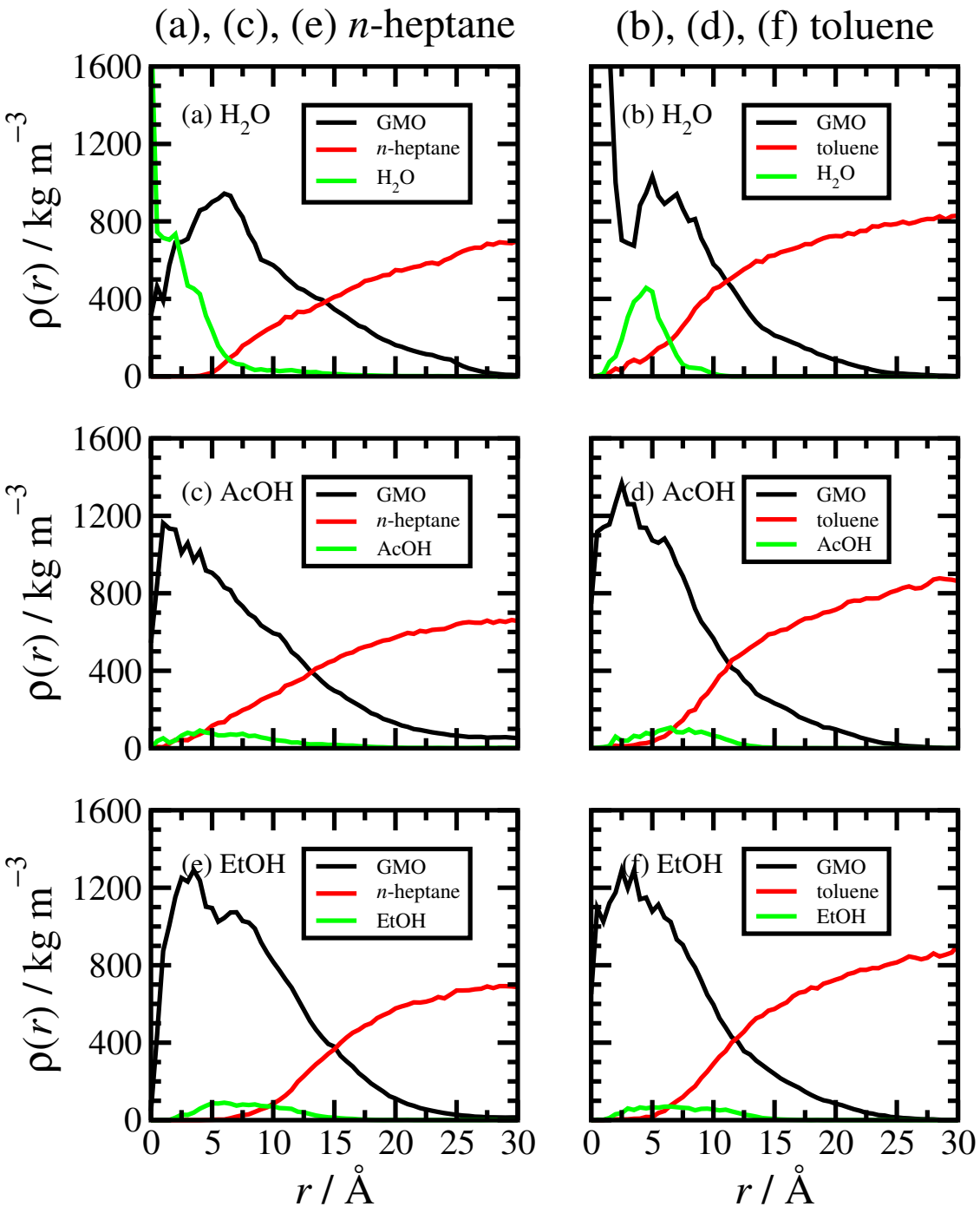


Figure 7: Mass density profiles $\rho(r)$ as functions of the radial distance $r$ from the RM center of mass for 20 wt% GMO systems in *n*-heptane (a, c, e) and toluene (b, d, f) with 1 wt% impurities ($H_2O$, AcOH, or EtOH): (a) and (b) $H_2O$; (c) and (d) AcOH; (e) and (f) EtOH.

# 4 Conclusions

In this work, computer simulations and small-angle neutron scattering have been used to study the formation of glycerol monooleate reverse micelles in *n*-heptane and toluene, either with or without small concentrations of impurities (water, acetic acid, or ethanol). It is found that reverse micelles can form on the simulation timescale (up to 10 ns) with glycerol monooleate concentrations of up to 20 wt%. From simulations, the typical dimensions (semi-axes) of the equivalent ellipsoids of the reverse micelles are found to be in the range 15–23 Å, and the radii of gyration lie are in the region of 15 Å. The radii of gyration extracted from neutron-scattering results are in good general agreement with the simulation results, but both sets of data give reverse-micelle dimensions marginally lower than those obtained from small-angle X-ray scattering studies.[14] At very high glycerol monooleate concentrations (up to 20 wt%) the average separation between the reverse micelles approaches the size of the simulation box, and so not much can be said about how the reverse micelles merge and form structures on larger lengthscales. Nonetheless, concentrations on the 1–10 wt% are more typical and relevant to applications, and under these conditions, distinct reverse micelles are clearly observed. Although reverse micelles in toluene contain smaller numbers of glycerol monooleate molecules than in *n*-heptane, the overall dimensions are similar due to greater toluene penetration and swelling. Glycerol monooleate is widely used as a friction modifier. The formation of reverse micelles is bound to have an effect on the friction-modification properties of the glycerol monooleate, and this is the subject of ongoing work.

## Associated Content

**Supporting Information Available:** Two molecular movies showing the formation of reverse micelles starting from disordered configurations of glycerol monooleate, solvent, and impurity. Movie 1 shows 10 wt% GMO in pure *n*-heptane without impurity. Movie 2 shows 10 wt% GMO in *n*-heptane with 1 wt% water. In each case, the simulated time is 20 ns, and the end result is a single, well-defined reverse micelle. The molecular representations are the same as in Figure 1 except that

in Movie 2 the added water is shown in blue to distinguish the water oxygens from the GMO oxygens. This material is available free of charge via the Internet at `http://pubs.acs.org`.

## Acknowledgement

This research was supported by Infineum UK Ltd through a PhD studentship to J.L.B.-S. and funds for the purchase of computer hardware.

## References

(1) Pileni, M.-P. Reverse Micelles as Microreactors. *J. Phys. Chem.* **1993**, *97*, 6961–6973.

(2) Chen, C.; Cook, O.; Nicholson, C. E.; Cooper, S. J. Leapfrogging Ostwald's Rule of Stages: Crystallization of Stable $\gamma$-Glycine Directly from Microemulsions. *Cryst. Growth. Des.* **2011**, *11*, 2228–2237.

(3) Petit, C.; Lixon, P.; Pileni, M.-P. In Situ Synthesis of Silver Nanocluster in AOT Reverse Micelles. *J. Phys. Chem.* **1993**, *97*, 12974–12983.

(4) Hopwood, J. D.; Mann, S. Synthesis of Barium Sulfate Nanoparticles and Nanofilaments in Reverse Micelles and Microemulsions. *Chem. Mater.* **1997**, *9*, 1819–1828.

(5) Ruckenstein, E.; Nagarajan, R. Aggregation of Amphiphiles in Nonaqueous Media. *J. Phys. Chem.* **1980**, *84*, 1349–1358.

(6) Eicke, H.-F.; Christen, H. Is Water Critical to the Formation of Micelles in Apolar Media?? *Helv. Chim. Acta* **1978**, *61*, 2258–2263.

(7) Wootton, A.; Picavez, F.; Harrowell, P. The Structure and Thermodynamic Stability of Reverse Micelles in Dry AOT/Alkane Mixtures. *AIP Conf. Proc.* **2008**, *982*, 289–294.

(8) Smith, G. N.; Brown, P.; Rogers, S. E.; Eastoe, J. Evidence for a Critical Micelle Concentration of Surfactants in Hydrocarbon Solvents. *Langmuir* **2013**, *29*, 3252–3258.

(9) Scartazzini, R.; Luisi, P. L. Organogels from Lecithins. *J. Phys. Chem.* **1988**, *92*, 829–833.

(10) Schurtenberger, P.; Scartazzini, R.; Magid, L. J.; Leser, M. E.; Luisi, P. L. Structural and Dynamic Properties of Polymer-like Reverse Micelles. *J. Phys. Chem.* **1990**, *94*, 3695–3701.

(11) Schurtenberger, P.; Magid, L. J.; King, S. M.; Lindner, P. Cylindrical Structure and Flexibility of Polymerlike Lecithin Reverse Micelles. *J. Phys. Chem.* **1991**, *95*, 4173–4176.

(12) Ibrahim, T. H.; Neuman, R. D. Nanostructure of Open Water-Channel Reversed Micelles. I. $^1$H NMR Spectroscopy and Molecular Modeling. *Langmuir* **2004**, *20*, 3114–3122.

(13) Pitzalis, P.; Monduzzi, M.; Krog, N.; Larsson, H.; Ljusberg-Wahren, H.; Nylander, T. Characterization of the Liquid-Crystalline Phases in the Glycerol Monooleate/Diglycerol Monooleate/Water System. *Langmuir* **2000**, *16*, 6358–6365.

(14) Shrestha, L. K.; Shrestha, R. G.; Abe, M.; Ariga, K. Reverse Micelle Microstructural Transformations Induced by Oil and Water. *Soft Matter* **2011**, *7*, 10017–10024.

(15) Kunieda, H.; Ozawa, K.; Huang, K.-L. Effect of Oil on the Surfactant Molecular Curvatures in Liquid Crystals. *J. Phys. Chem. B* **1998**, *102*, 831–838.

(16) Shrestha, R. G.; Shrestha, L. K.; Ariga, K.; Abe, M. Reverse Micelle Microstructural Transformations Induced by Surfactant Molecular Structure, Concentration, and Temperature. *J. Nanosci. Nanotechno.* **2011**, *11*, 7665–7675.

(17) Shrestha, L. K.; Glatter, O.; Aramaki, K. Structure of Nonionic Surfactant Glycerol $\alpha$-Monomyristate Micelles in Organic Solvents: A SAXS Study. *J. Phys. Chem. B* **2009**, *113*, 6290–6298.

(18) Shrestha, L. K.; Shrestha, R. G.; Aramaki, K.; Hill, J. P.; Ariga, K. Nonionic Reverse Micelle Formulation and Their Microstructure Transformations in an Aromatic Solvent Ethylbenzene. *Colloids Surf. A* **2012**, *414*, 140–150.

(19) Rappolt, M.; Cacho-Nerin, F.; Morello, C.; Yaghmur, A. How the Chain Configuration Governs the Packing of Inverted Micelles in the Cubic *Fd3m*-Phase. *Soft Matter* **2013**, *9*, 6291–6300.

(20) Brown, D.; Clarke, J. H. R. Molecular Dynamics Simulation of a Model Reverse Micelle. *J. Phys. Chem.* **1988**, *92*, 2881–2888.

(21) Abel, S.; Sterpone, F.; Bandyopadhyay, S.; Marchi, M. Molecular Modeling and Simulations of AOT-Water Reverse Micelles in Isooctane: Structural and Dynamic Properties. *J. Phys. Chem. B* **2004**, *108*, 19458–19466.

(22) Abel, S.; Waks, M.; Urbach, W.; Marchi, M. Structure, Stability, and Hydration of a Polypeptide in AOT Reverse Micelles. *J. Am. Chem. Soc.* **2006**, *128*, 382–383.

(23) Chowdhary, J.; Ladanyi, B. M. Molecular Dynamics Simulation of Aerosol-OT Reverse Micelles. *J. Phys. Chem. B* **2009**, *113*, 15029–15039.

(24) Vasquez, V. R.; Williams, B. C.; Graeve, O. A. Stability and Comparative Analysis of AOT/Water/Isooctane Reverse Micelle System Using Dynamic Light Scattering and Molecular Dynamics. *J. Phys. Chem. B* **2011**, *115*, 2979–2987.

(25) Nevidimov, A. V.; Razumov, V. F. Molecular Dynamics Simulations of AOT Reverse Micelles' Self-assembly. *Mol. Phys.* **2009**, *107*, 2169–2180.

(26) Chaitanya, V. S. V.; Senapati, S. Self-Assembled Reverse Micelles in Supercritical $CO_2$ Entrap Protein in Native State. *J. Am. Chem. Soc.* **2008**, *130*, 1866–1870.

(27) Linse, P. Molecular Dynamics Study of the Aqueous Core of a Reversed Ionic Micelle. *J. Chem. Phys.* **1989**, *90*, 4992–5004.

(28) Linse, P.; Halle, B. Counterion N.M.R. in Heterogeneous Aqueous Systems. A Molecular Dynamics Simulation Study of the Electric Field Gradient. *Mol. Phys.* **1989**, *67*, 537–573.

(29) Faeder, J.; Ladanyi, B. M. Molecular Dynamics Simulations of the Interior of Aqueous Reverse Micelles. *J. Phys. Chem. B* **2000**, *104*, 1033–1046.

(30) Faeder, J.; Ladanyi, B. M. Solvation Dynamics in Aqueous Reverse Micelles: A Computer Simulation Study. *J. Phys. Chem. B* **2001**, *105*, 11148–11158.

(31) Faeder, J.; Albert, M. V.; Ladanyi, B. M. Molecular Dynamics Simulations of the Interior of Aqueous Reverse Micelles: A Comparison between Sodium and Potassium Counterions. *Langmuir* **2003**, *19*, 2514–2520.

(32) Faeder, J.; Ladanyi, B. M. Solvation Dynamics in Reverse Micelles: The Role of Headgroup-Solute Interactions. *J. Phys. Chem. B* **2005**, *109*, 6732–6740.

(33) Harpham, M. R.; Ladanyi, B. M.; Levinger, N. E. The Effect of the Counterion on Water Mobility in Reverse Micelles Studied by Molecular Dynamics Simulations. *J. Phys. Chem. B* **2005**, *109*, 16891–16900.

(34) Rosenfeld, D. E.; Schmuttenmaer, C. A. Dynamics of Water Confined Within Reverse Micelles. *J. Phys. Chem. B* **2006**, *110*, 14304–14312.

(35) LAMMPS Molecular Dynamics Simulator. http://lammps.sandia.gov.

(36) Plimpton, S. J. Fast Parallel Algorithms for Short-Range Molecular Dynamics. *J. Comp. Phys.* **1995**, *117*, 1–19.

(37) Packmol. http://www.ime.unicamp.br/ martinez/packmol/.

(38) Martínez, L.; Andrade, R.; Birgin, E. G.; Martínez, J. M. PACKMOL: A Package for Building Initial Configurations for Molecular Dynamics Simulations. *J. Comp. Chem.* **2009**, *30*, 2157–2164.

(39) Mayo, S. L.; Olafson, B. D.; Goddard III, W. A. DREIDING: A Generic Force Field for Molecular Simulations. *J. Phys. Chem.* **1990**, *94*, 8897–8909.

(40) Jorgensen, W. L.; Maxwell, D. S.; Tirado-Rives, J. Development and Testing of the OPLS All-Atom Force Field on Conformational Energetics and Properties of Organic Liquids. *J. Am. Chem. Soc.* **1996**, *118*, 11225–11236.

(41) Siu, S. W. I.; Pluhackova, K.; Böckmann, R. A. Optimization of the OPLS-AA Force Field for Long Hydrocarbons. *J. Chem. Theory Comput.* **2012**, *8*, 1459–1470.

(42) Martin, M. G.; Siepmann, J. I. Transferable Potentials for Phase Equilibria. 1. United-Atom Description of *n*-Alkanes. *J. Phys. Chem. B* **1998**, *102*, 2569–2577.

(43) Chen, B.; Siepmann, J. I. Transferable Potentials for Phase Equilibria. 3. Explicit-Hydrogen Description of Normal Alkanes. *J. Phys. Chem. B* **1999**, *103*, 5370–5379.

(44) Wick, C. D.; Martin, M. G.; Siepmann, J. I. Transferable Potentials for Phase Equilibria. 4. United-Atom Description of Linear and Branched Alkenes and Alkylbenzenes. *J. Phys. Chem. B* **2000**, *104*, 8008–8016.

(45) NIST Chemistry WebBook. http://webbook.nist.gov/chemistry/.

(46) Frisch, M. J.; Trucks, G. W.; Schlegel, H. B.; Scuseria, G. E.; Robb, M. A.; Cheeseman, J. R.; Scalmani, G.; Barone, V.; Mennucci, B.; Petersson, G. A.; Nakatsuji, H.; Caricato, M.; Li, X.; Hratchian, H. P.; Izmaylov, A. F.; Bloino, J.; Zheng, G.; Sonnenberg, J. L.; Hada, M.; Ehara, M.; Toyota, K.; Fukuda, R.; Hasegawa, J.; Ishida, M.; Nakajima, T.; Honda, Y.; Kitao, O.; Nakai, H.; Vreven, T.; Montgomery, Jr., J. A.; Peralta, J. E.; Ogliaro, F.; Bearpark, M.; Heyd, J. J.; Brothers, E.; Kudin, K. N.; Staroverov, V. N.; Kobayashi, R.; Normand, J.; Raghavachari, K.; Rendell, A.; Burant, J. C.; Iyengar, S. S.; Tomasi, J.; Cossi, M.; Rega, N.; Millam, J. M.; Klene, M.; Knox, J. E.; Cross, J. B.; Bakken, V.; Adamo, C.; Jaramillo, J.; Gomperts, R.; Stratmann, R. E.; Yazyev, O.; Austin, A. J.; Cammi, R.; Pomelli, C.; Ochterski, J. W.; Martin, R. L.; Morokuma, K.; Zakrzewski, V. G.; Voth, G. A.; Salvador, P.; Dannenberg, J. J.; Dapprich, S.; Daniels, A. D.; Farkas, Ã.; Foresman, J. B.; Ortiz, J. V.; Cioslowski, J.; Fox, D. J. Gaussian 09. 2009; Gaussian, Inc., Wallingford, CT.

(47) Glinka, C. J.; Barker, J. G.; Hammouda, B.; Krueger, S.; Moyer, J. J.; Orts, W. J. The 30 m Small-Angle Neutron Scattering Instruments at the National Institute of Standards and Technology. *J. Appl. Cryst.* **1998**, *31*, 430–445.

(48) Theodorou, D. N.; Suter, U. W. Shape of Unperturbed Linear Polymers: Polypropylene. *Macromolecules* **1985**, *18*, 1206–1214.

(49) Lee, H.; Baker, Jr., J. R.; Larson, R. G. Molecular Dynamics Studies of the Size, Shape, and Internal Structure of 0% and 90% Acetylated Fifth-Generation Polyamidoamine Dendrimers in Water and Methanol. *J. Phys. Chem. B* **2006**, *110*, 4014–4019.

(50) Dougan, L.; Bates, S. P.; Hargreaves, R.; Fox, J. P.; Crain, J.; Finney, J. L.; Réat, V.; Soper, A. K. Methanol-Water Solutions: A Bi-Percolating Liquid Mixture. *J. Chem. Phys.* **2004**, *121*, 6456–6462.

(51) Allison, S. K.; Fox, J. P.; Hargreaves, R.; Bates, S. P. Clustering and Microimmiscibility in Alcohol-Water Mixtures: Evidence from Molecular-Dynamics Simulations. *Phys. Rev. B* **2005**, *71*, 024201.

(52) Dougan, L.; Hargreaves, R.; Bates, S. P.; Finney, J. L.; Réat, V.; Soper, A. K.; Crain, J. Segregation in Aqueous Methanol Enhanced by Cooling and Compression. *J. Chem. Phys.* **2005**, *122*, 174514.

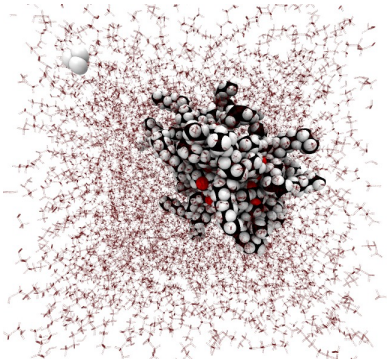

For Table of Contents Only